

—Supporting Information—

**Polystyrene Nano- and Microplastic Accumulation at
Arabidopsis and Wheat Root Cap Cells, but No Evidence for
Uptake into Roots**

Stephen E. Taylor^{a,b}, Carolyn I. Pearce^b, Karen A. Sanguinet^a, Dehong Hu^c, William
B. Chrisler^c, Young-Mo Kim^c, Zhan Wang^d, Markus Flury^{a,e}

^a*Department of Crop & Soil Sciences, Washington State University, Pullman, WA 99164,
USA*

^b*Energy and Environment Directorate, Pacific Northwest National Laboratory, Richland, WA
99352, USA*

^c*Earth and Biological Sciences Directorate, Pacific Northwest National Laboratory, Richland,
WA 99352, USA*

^d*College of Land and Environment, Shenyang Agricultural University, Shenyang, China*

^e*Department of Crop & Soil Sciences, Washington State University, Puyallup, WA 98371,
USA*

Supporting information includes details on experimental protocols, confocal images of method
validation, confocal images of root cross-sections, SEM images of polystyrene beads.

S1 Confocal Microscopy

Each focal plane in the confocal z-stacks was examined for evidence of plastic uptake into the plant cells. A 20X magnification and NA 0.5 objective was used for wheat samples. A 40X magnification, NA 1.1 objective was used for Arabidopsis samples. Calcofluor counterstaining was imaged with 405 nm excitation and a 410–497 nm emission detector. Propidium iodide staining was imaged with 561 nm excitation and a 566–718 nm emission detector. The intensity of the fluorescence of the 40 nm and 1 μm polystyrene spheres was different; therefore, two sets of settings at high and low overall sensitivities were used to detect the fluorescence from the particles. The high sensitivity settings include stronger laser power, a wider fluorescence spectrum range (493–582 nm), and higher detector gain. The low sensitivity settings include lower laser power, a narrower fluorescence spectrum range (493–555 nm), and lower detector gain. The microscope settings (gain, emission detection range, laser intensity, magnification, see Table S1) were kept the same between treatments for each species to prevent any false-positive identification of fluorescent microspheres from other auto-fluorescent molecules in or on the plant cells.

S2 Validation of Confocal Microscopy

Figure S2 shows confocal images for the nano- and microspheres in growth medium and a wheat root grown without polystyrene spheres. The images show that both 40 nm and 1 μm plastic spheres could be imaged and that the laser and microscope settings were optimized for imaging the polystyrene spheres. By using both the broader range and higher laser strength and the lower intensity setting with narrower detection range, it was confirmed that fluorescence observed in the broader range/higher laser intensity track were 40 nm plastic

particles, and not background fluorescence.

The 40 nm and 1 μm plastic spheres were present in the growth medium as both single particles and aggregates. The signal of the 40 nm spheres was faint, especially with the lower intensity/narrower range detector, but still visible. Calcofluor and propidium iodide staining was used to stain cell walls. The autofluorescence of the roots is much weaker than the fluorescence of the calcofluor and propidium iodide counter-stain and polystyrene particles at the same wavelength band.

We also tested for potential quenching of fluorescence of the fluorescently-labeled spheres due to autoclaving and pH variations close to the root surfaces. Fluorescently-labeled spheres were placed in a 1/4 strength Hoagland solution at pH ranging from 3 to 10 for 48 hours, autoclaved, spun down to remove all particles, and the supernatant tested for fluorescence at 488 nm excitation wavelength. Fluorescence was observed in the 40 nm supernatant, indicating some leaching of the fluorescent dye after treatment, which decreased as pH increased. This is most likely caused by spheres remaining in the supernatant after centrifugation. However, the overall strength fluorescence of the spheres remained intact (Figure S3A,B). Additionally, confocal images of the particles after autoclaving showed no evidence of quenching (Figure S3C,D), and scanning electron microscopy images showed that the particles maintained their shape and size in the agar growth media after the autoclaving procedure (Figure S4).

S3 Pyrolysis GC-MS

Pyrolysis GC-MS was performed with a CDS Analytical Pyroprobe (filament pyrolyzer) with a 500 Pyrolysis Injection probe at 500 °C (CDS Analytical, Oxford, PA). The pyrolyzer was attached to an Agilent 6890N gas chromatograph with an HP-5MS column linked to an

Agilent 5975B mass selective detector (Agilent Technologies, Santa Clara, CA). Mass spectra from peaks were compared to the NIST17/WILEY 11 GCMS spectral library.

Plant roots of Arabidopsis plants and wheat were washed three times (phosphate-buffered saline (PBS) with 1% Triton x-100), vortexed for 30 seconds, and sonicated for 5 minutes. Washed plant material was completely dried and weighed. The entire Arabidopsis plant (~ 0.2 mg) and a 2-cm section of the wheat root including the tip (~ 0.2 mg) were placed into a glass pyrolysis tube for pyrolysis and measurements.

To differentiate between background and polystyrene sphere signal, peak areas were normalized by dividing by the mass of plant material used for pyrolysis, and then average peak area of the three replications was calculated for each treatment. Styrene peak area ratios for treatments to negative controls (treatment:control) were found to be 0.45 and 0.73 for the 40 nm and 1 μm treatments for wheat, respectively. For Arabidopsis, peak area ratios for treatment to negative control were 1.02 and 0.76 for the 40 nm and 1 μm treatments respectively. This data would suggest that the styrene peak is the same or stronger in the negative control than in the treatment. However, peak area had large variability between replications for each treatment, including negative controls (CV from 11.9% to 79.7%). Peak area calculations were performed for two other polystyrene degradation products (3-butene-1,3,-diyltribenzene and 5-hexene-1,3,5-triyltribenzene) with similar results to the styrene monomer.

This amount of variability between replications indicates that plant material is the major source of styrene monomers in the pyrolysis degradation products. Peak ratio calculations, therefore, are not conclusive about the presence or absence of polystyrene particles in the plant roots. Any polystyrene that was left on the root surface after the washing procedure (Figure 5) was not significant enough to overcome the variability in naturally occurring plant material whose thermal degradation products overlap with those of polystyrene.

Pyrolysis GC-MS is a method commonly used to characterize organic molecules and to characterize plant material.^{1,2} GC-MS methods have been used to identify the presence of Chlorpyrifos³ and amino acids⁴ in plant material. The technique has also been used to identify microplastics in seawater, beach sediments, and marine organisms.⁵ It has not yet, to our knowledge, been used to determine uptake of other carbon materials in plants. Thermal degradation products of plant materials as well as detection limits may restrict the pyrolysis GC-MS method for analysis of plastic nanoparticles in plants (see discussion in main manuscript).

Alternative and complementary analysis techniques are UV/vis⁶ and Raman⁷ spectroscopy, and isotope labeling (C-13 or C-14).^{8,9} UV/vis spectroscopy in combination with chemical digestion has recently been used to determine the presence of carbon nanotubes in lettuce,⁶ and isotopically labeled plastic particles could be used to investigate uptake and translocation.⁹ The detection limit for the UV/vis method for carbon nanotubes has been reported as 0.019–0.18 $\mu\text{g mg}^{-1}$ for root tissue.⁶ This corresponds to a detection limit of 0.004 to 0.036 μg , when compared to a Pyrolysis GC-MS analysis (assuming a sample mass of 0.2 mg in the pyrolysis tube as used in our experiments). The detection limit of a Raman microscope for carbon tube analysis in plant tissue was reported⁷ as 0.025 $\mu\text{g mg}^{-1}$, a resolution in the lower range of the UV/vis technique.

Literature Cited

- (1) Ralph, J.; Hatfield, R. D. Pyrolysis-GC-MS characterization of forage materials. *Journal of Agricultural and Food Chemistry* **1991**, *39*, 1426–1437.
- (2) van Erven, G.; de Visser, R.; Merkx, D. W. H.; Strolenberg, W.; de Gijssel, P.; Gruppen, H.; Kabel, M. A. Quantification of lignin and its structural features in plant biomass using ^{13}C lignin as internal standard for pyrolysis-GC-SIM-MS. *Analytical Chemistry* **2017**, *89*, 10907–10916.
- (3) Yu, X.-Y.; Ying, G.-G.; Kookana, R. S. Reduced plant uptake of pesticides with biochar additions to soil. *Chemosphere* **2009**, *76*, 665–671.
- (4) Persson, J.; Näsholm, T. A GC-MS method for determination of amino acid uptake by plants. *Physiologia Plantarum* **2001**, *113*, 352–358.
- (5) Hermabessiere, L.; Himber, C.; Boricaud, B.; Kazour, M.; Amara, R.; Cassone, A.-L.; Laurentie, M.; Paul-Pont, I.; Soudant, P.; Dehaut, A.; Duflos, G. Optimization, performance, and application of a pyrolysis-GC/MS method for the identification of microplastics. *Anal. Bioanal. Chem.* **2018**, *410*, 6663–6676.
- (6) Das, K. K.; Nava, V.; Chang, C.-W.; Chan, J. W.; Xing, B.; Yang, Y. Emerging investigator series: quantification of multiwall carbon nanotubes in plant tissues with spectroscopic analysis. *Environmental Science: Nano* **2019**, *6*, 380–387.
- (7) Das, K. K.; You, Y.; Torres, M.; Masias-Barrios, F.; Wang, X.; Tao, S.; Xing, B.; Yang, Y. Development and application of a digestion-Raman analysis approach for studying multiwall carbon nanotube uptake in lettuce. *Environmental Science: Nano* **2018**, *5*, 659–668.

- (8) Zhao, Q.; Ma, C.; White, J. C.; Dhankher, O. P.; Zhang, X.; Zhang, S.; Xing, B. Quantitative evaluation of multi-wall carbon nanotube uptake by terrestrial plants. *Carbon* **2017**, *114*, 661–670.
- (9) Larue, C.; Pinault, M.; Czarny, B.; Geogin, D.; Jaillard, D.; Bendiab, N.; Mayne-L'Hermite, M.; Taran, F.; Dive, V.; Carrière, M. Quantitative evaluation of multi-walled carbon nanotube uptake in wheat and rapeseed. *Journal of Hazardous Material* **2012**, *227–228*, 155–163.

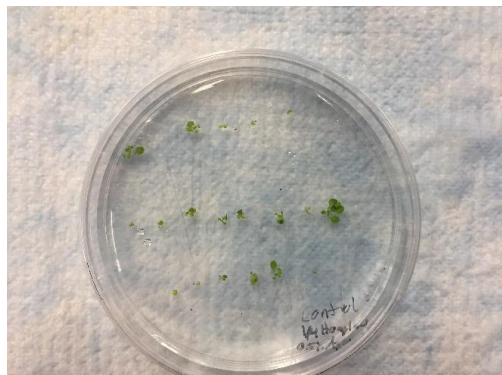
Table S1: Laser scanning confocal microscope settings for each nano- and microsphere treatment. All images were taken with a 20 \times objective for wheat and 40 \times objective for Arabidopsis. Control treatment without fluorescent spheres was also analyzed for each plant part at the same settings as shown in the table.

Treatment	Plant Species	Plant Part Examined	Excitation (nm)	Emission Detector (nm)
40 nm	Arabidopsis	Root Stem	488	493–555, 493–582
	Wheat	Root Stem		
1 μ m	Arabidopsis	Root Stem	488	493–555, 493–582
	Wheat	Root Stem		
All	All	Root Stem	405	410–497
40 nm	Arabidopsis	Root	561	566–718

Table S2: Summary of experimental settings for pyrolysis GC-MS.

Pyrolyzer	CDS Analytical Pyroprobe 500	Pyrolysis Injection Probe
Carrier Gas		Helium
Temperature		500 $^{\circ}$ C
Pyrolysis Time		1.0 minute
Transfer Line Temperature		250 $^{\circ}$ C
Gas Chromatograph		Agilent 6890N
Injector		Split-Splitless
Mode		Split 50:1
Temperature		250 $^{\circ}$ C
Column		HP-5MS 30m \times 250 μ m \times 0.25 μ m
Flow		1ml/ min
Temperature Program		40 $^{\circ}$ C hold for 1 min \rightarrow 280 $^{\circ}$ C @ 6 $^{\circ}$ C/min and hold for 15 min
Transfer Line Temperature		280 $^{\circ}$ C
Mass Spectrometer		Agilent 5975B Mass Selective Detector
Ionization Energy		70 eV
Scan Rate		4 scans/sec
Scan Range		45–400

(A) Control Arabidopsis (no plastic)



(D) Control Wheat (no plastic)



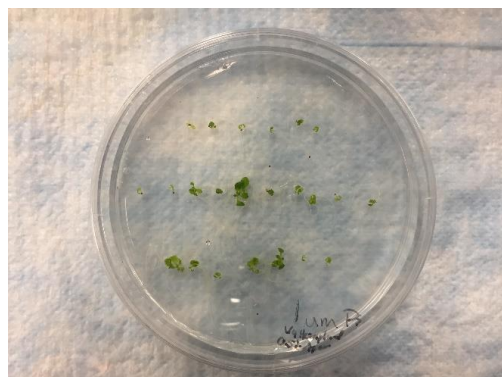
(B) Arabidopsis (40 nm spheres)



(E) Wheat (40 nm spheres)



(C) Arabidopsis (1.0 μm spheres)



(F) Wheat (1.0 μm spheres)



Figure S1: Images of Arabidopsis (A-C) and wheat plants (D-F) grown in sterile Petri Dishes with autoclaved 0.5% agar, one-fourth strength Hoagland solution, and associated plastic particle treatments listed in headings.

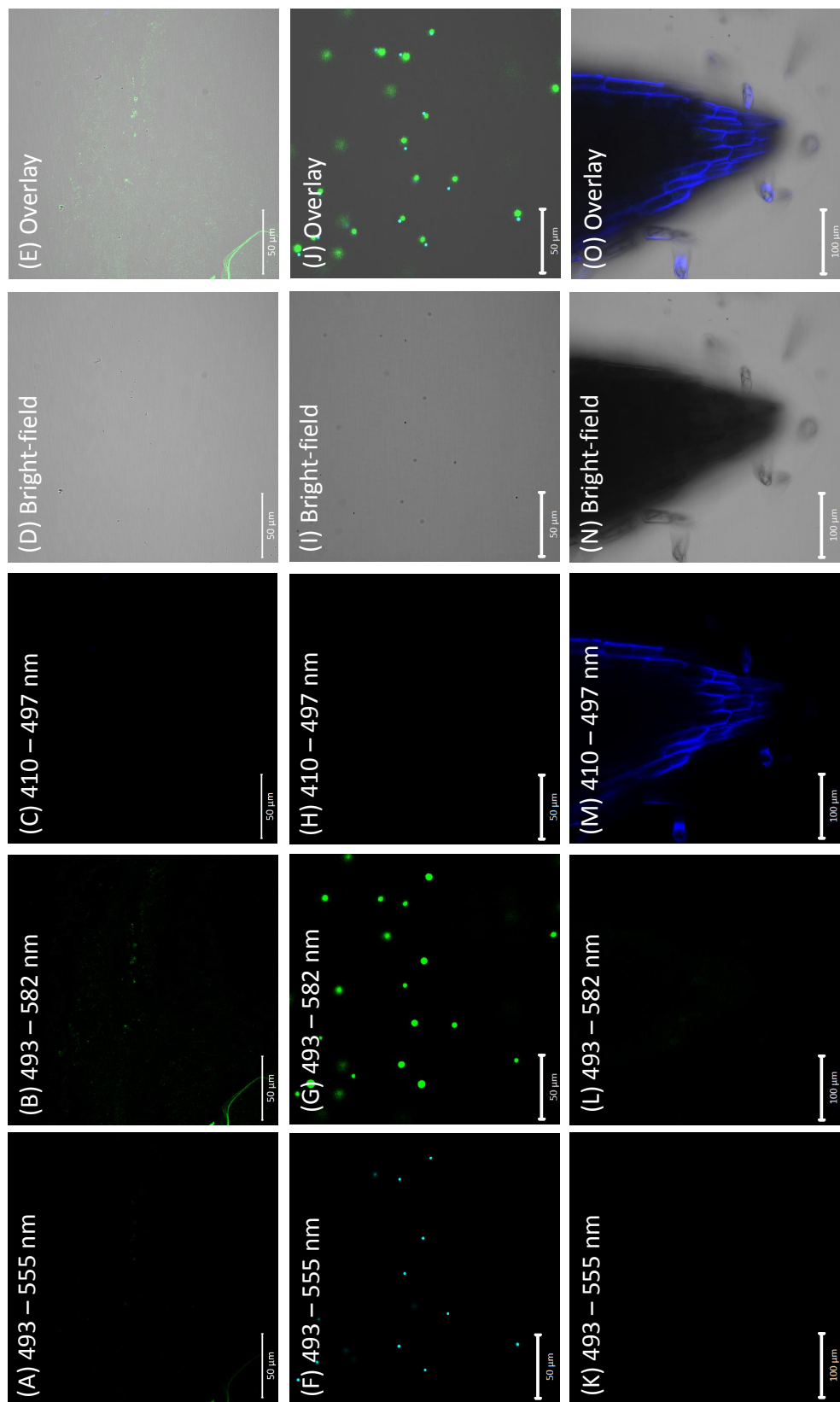


Figure S2: Confocal images of 40 nm (A-E), 1 μm (F-J) fluorescent polystyrene spheres, and no-spheres (K-O) control wheat roots, all images in agar. All detection channels are split into individual images, and finally overlaid (far-right). The 493–555 nm and 493–582 nm detection range allowed for confirmation that the particles in the image were fluorescent spheres and not auto-fluorescent particles in the plant. The 410–497 nm detection range was for the calcofluor white stain.

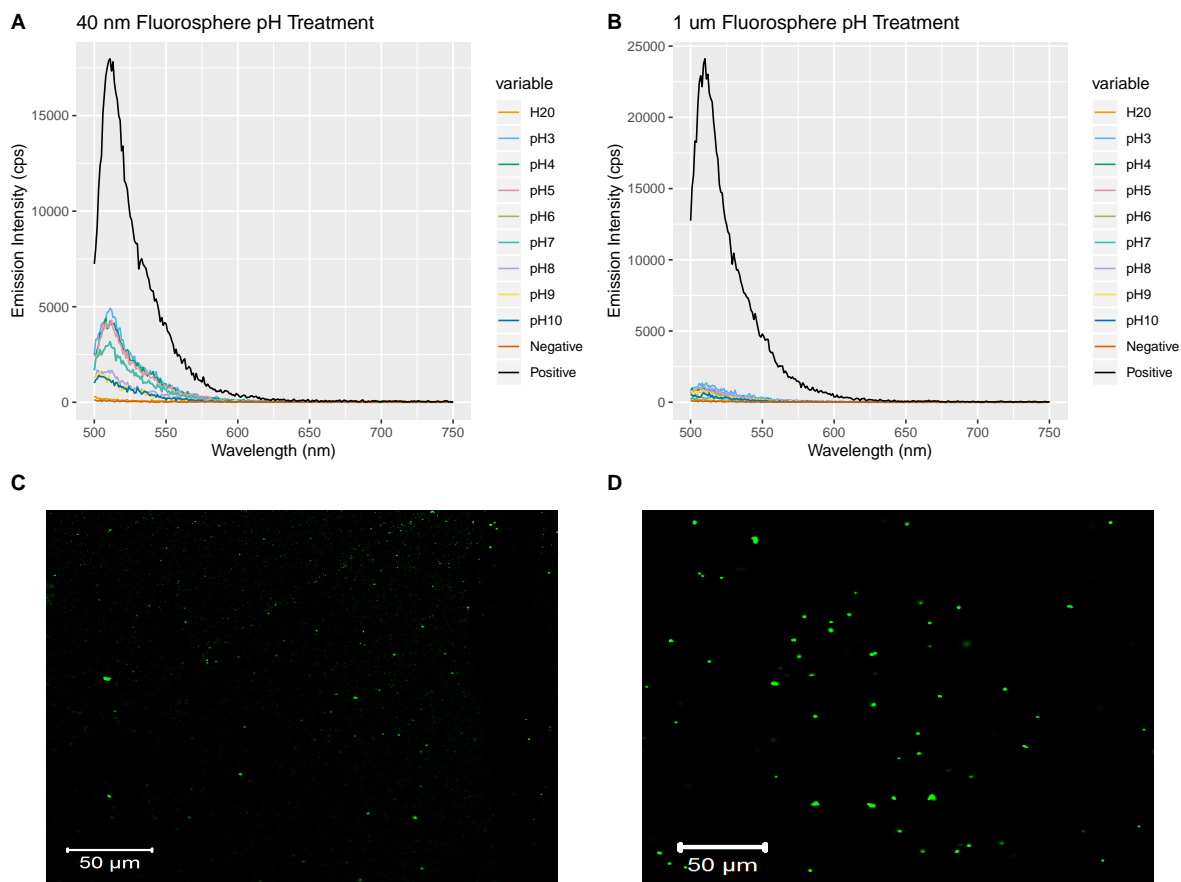


Figure S3: (A,B) Spectra of 40 nm and 1 μm fluorescently-labeled spheres at excitation wavelength of 488 nm. Black line is the suspended spheres (positive control), and colored lines are spectra of the supernatant at different pH after autoclaving and centrifugation of the suspensions. (C,D) Confocal images of 40 nm and 1 μm fluorescently-labeled spheres after autoclaving.

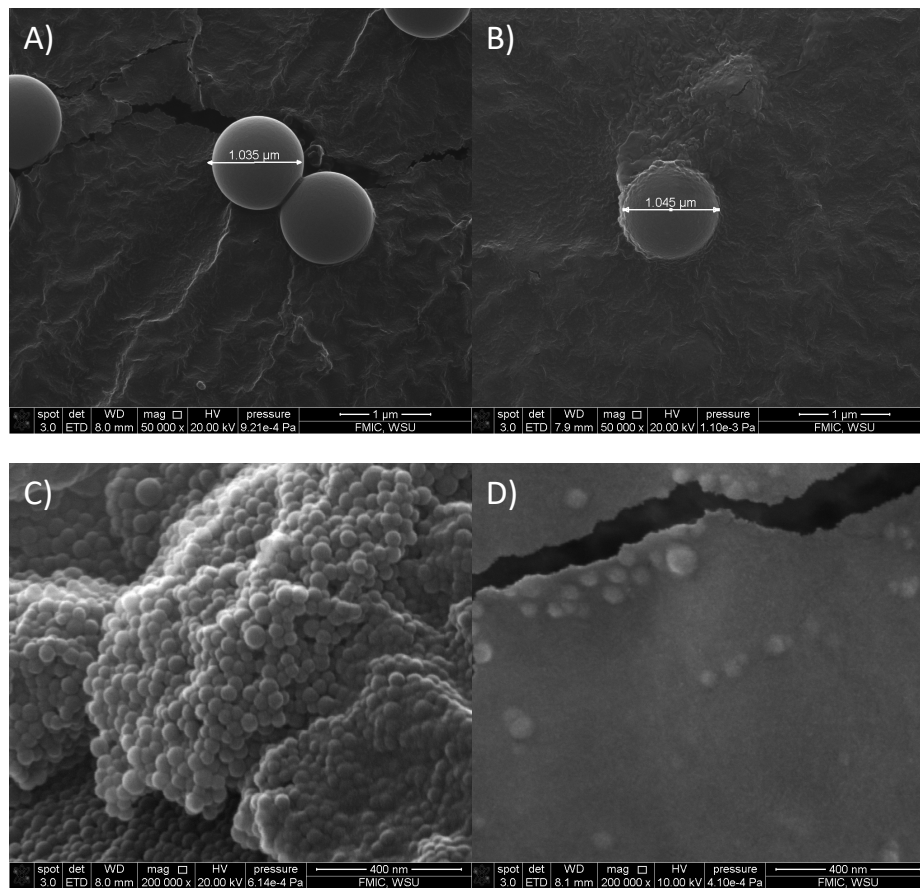


Figure S4: Scanning electron microscopy images of 1 μm and 40 nm polystyrene spheres (A,C) before autoclaving and (B,D) after autoclaving in growth media. Images show that autoclaving did not affect size or shape of the plastic particles.

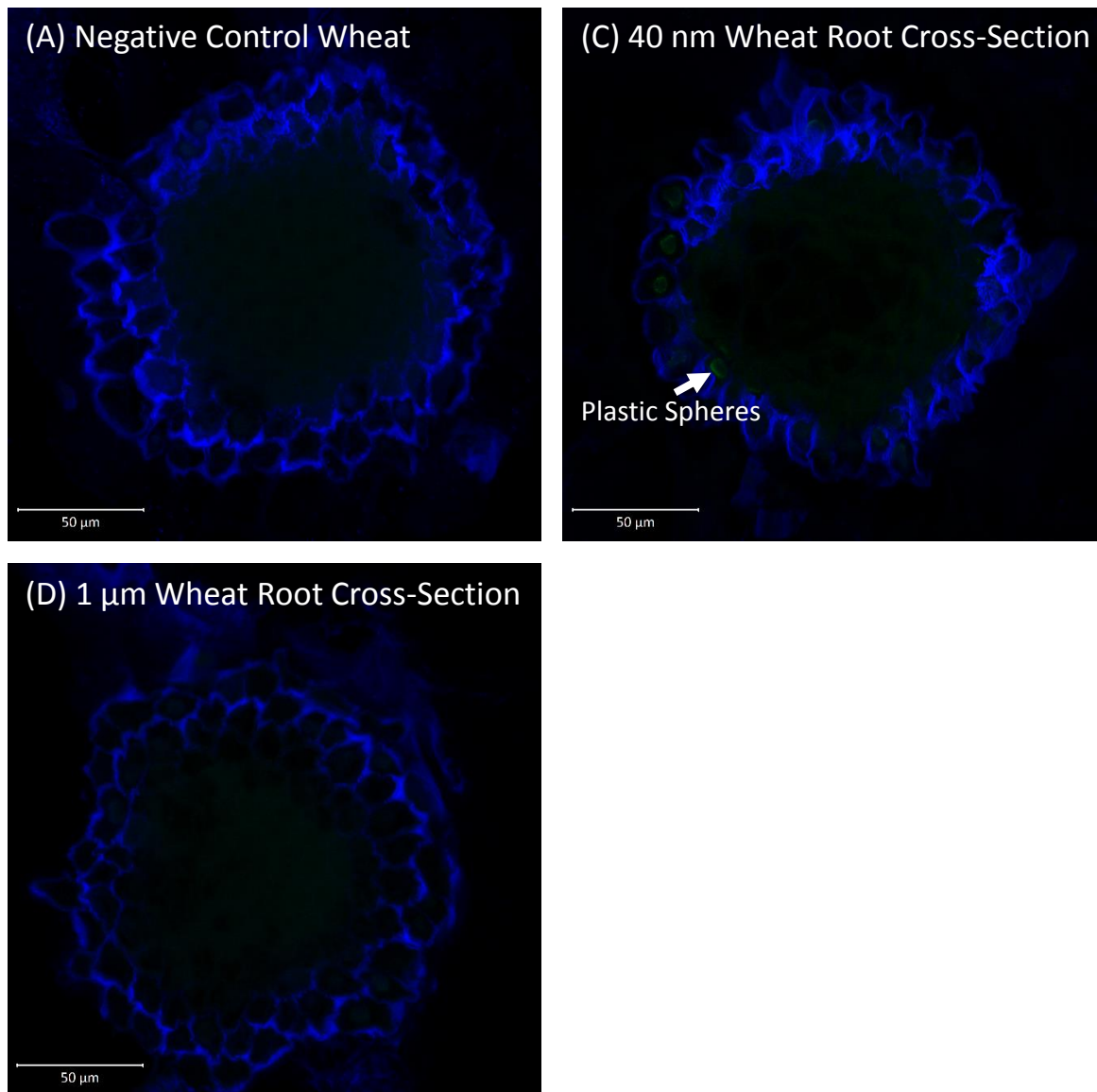


Figure S5: Images of wheat root cross-sections of the pre-differentiated zone of the root tip. All images show root epidermal cells with calcofluor staining. Image C (arrow) shows evidence for 40 nm polystyrene spheres inside root cells that are likely root cap cells.

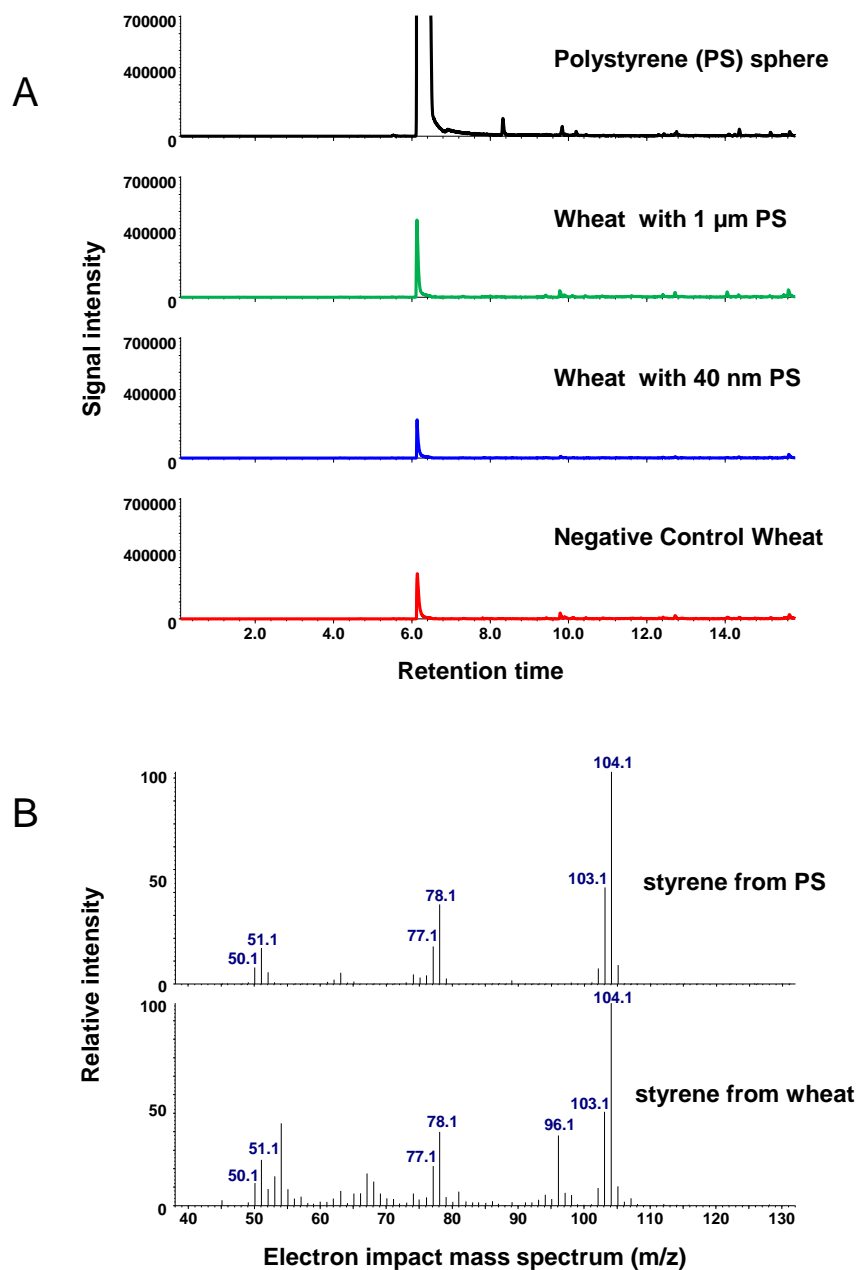


Figure S6. (A) Extracted ion chromatogram of styrene from Pyrolysis GC-MS for wheat. A unique mass fragment of 104 m/z was selected to plot chromatograms from polystyrene spheres (top), wheat grown without polystyrene spheres (bottom), and wheat grown with polystyrene spheres (middle two). The thermal degradation product styrene was detected from both control and polystyrene-exposed samples. (B) MS spectra of thermal hydrolyzed styrene. Electron impacted mass fragments are shown from polystyrene standard (top) and wheat with polystyrene.

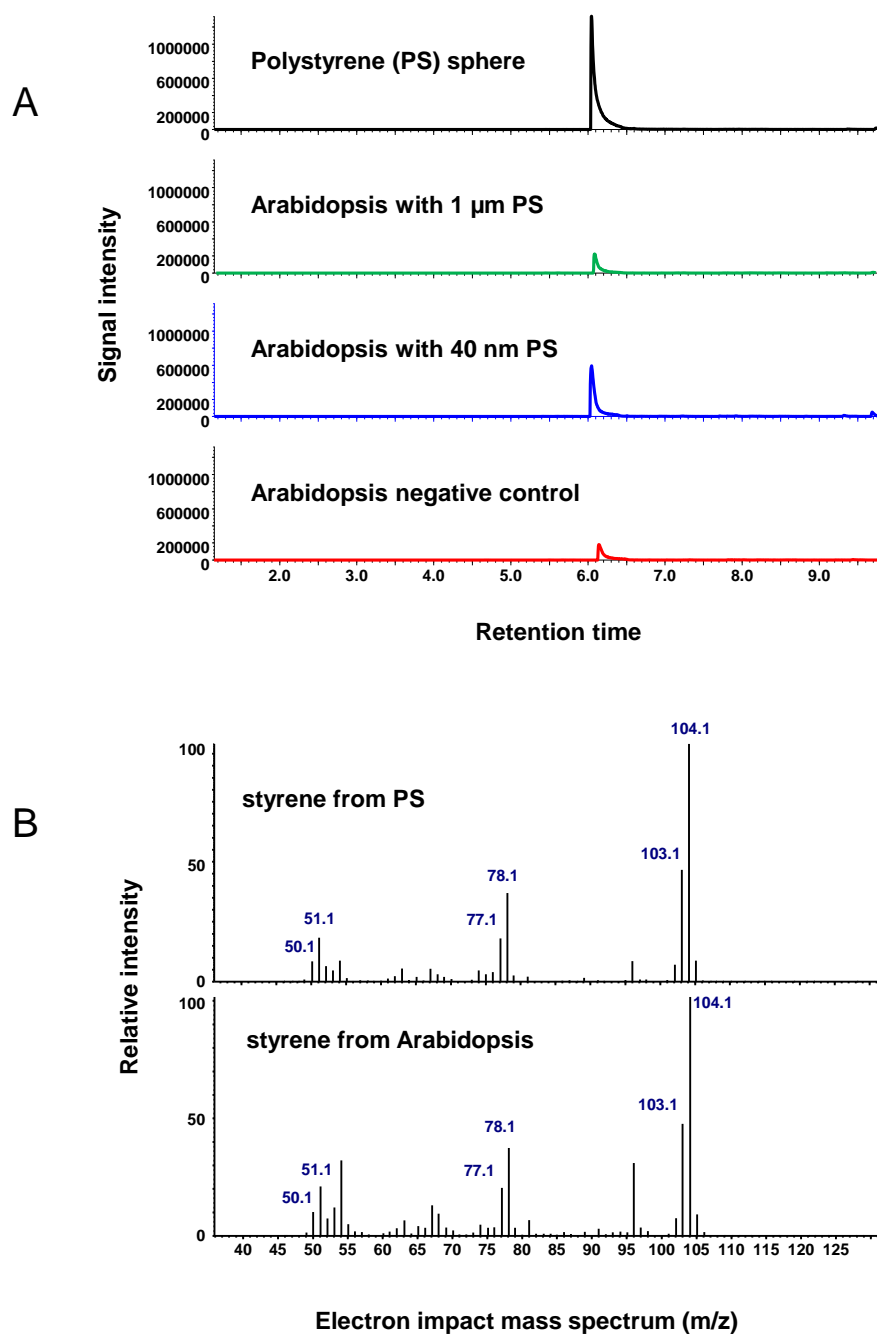


Figure S7. (A) Extracted ion chromatogram of styrene from Pyrolysis GC-MS for Arabidopsis. A unique mass fragment of 104 m/z was selected to plot chromatograms from polystyrene spheres (top), Arabidopsis grown without polystyrene spheres (bottom), and Arabidopsis grown with polystyrene spheres (middle two). The thermal degradation product styrene was detected from both control and polystyrene-exposed samples. (B) MS spectra of thermal hydrolyzed styrene. Electron impacted mass fragments are shown from polystyrene standard (top) and Arabidopsis polystyrene.